

www.acsami.org Research Article

Effects of Mesoporosity and Conductivity of Hierarchically Porous Carbon Supports on the Deposition of Pt Nanoparticles and Their Performance as Electrocatalysts for Oxygen Reduction Reaction in Alkaline Media

Georgia Potsi, Yu-Han Joseph Tsai, Austin Reese, Dasol Yoon, Jeremy L. Hitt, Antonios Kouloumpis, Jin Suntivich, David A. Muller, Thomas E. Mallouk, and Emmanuel P. Giannelis*



Cite This: ACS Appl. Mater. Interfaces 2023, 15, 33028-33036



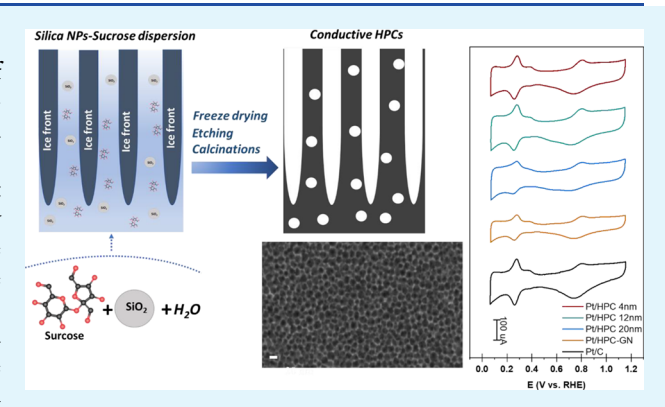
ACCESS I

III Metrics & More

Article Recommendations

s Supporting Information

ABSTRACT: The structural characteristics of supports, such as surface area and type of porosity, affect the deposition of electrocatalysts and greatly influence their electrochemical performance in fuel cells. In this work, we use a series of high surface area hierarchical porous carbons (HPCs) with defined mesoporosity as model supports to study the deposition mechanism of Pt nanoparticles. The resulting electrocatalysts are characterized by several analytical techniques, and their electrochemical performance is compared to a state-of-the-art, commercial Pt/C system. Despite the similar chemical composition and surface area of the supports, as well as similar amounts of Pt precursor used, the size of the deposited Pt nanoparticles varies, and it is inversely proportional to the mesopore size of the system. In addition, we show that an increase in the size of the catalyst particles can increase the specific activity of



the oxygen reduction reaction. We also report on our efforts to improve the overall performance of the above electrocatalyst systems and show that increasing the electronic conductivity of the carbon support by the addition of highly conductive graphene sheets improves the overall performance of an alkaline fuel cell.

KEYWORDS: support, carbon, mesoporous, conductivity, electrocatalyst

■ INTRODUCTION

The impact on climate from the use of fossil fuels has driven researchers to explore more environmentally friendly energy resources. Fuel cells have emerged as a sustainable approach for energy conversion applications in transportation, distributed heat and power generation, and energy storage systems.^{1,2} Electrocatalysts represent a critical component of fuel cells. As such they need to realize specific design criteria, including chemical and physical stability, high electronic conductivity, and specific structural characteristics that include high surface area and porosity.^{3,4} While the high surface area of supports enables the homogeneous deposition of electrocatalyst particles,⁵ the type of porosity also influences the overall performance by controlling the mass-transport properties, such as gas transport to the reactive sites, and ion transport within the ionomer network.3 Studies have shown that internal porosity contributes to the homogeneous distribution of the catalyst particles and protects the nanoparticles from ionomer adsorption, which lowers their activity.6 In addition, the retention of electrochemically active surface area (ECSA) tends to improve with increasing porosity of the support.

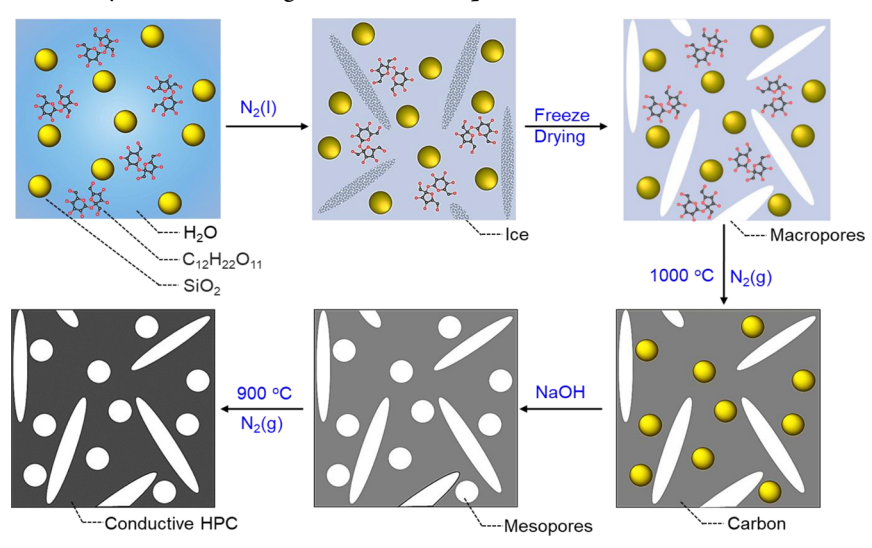
Carbon black, e.g. Vulcan carbon, is one of the most widely used carbon supports in fuel cells due to its ease of fabrication, electrical conductivity, and surface area. 4,5,8-10 Despite the beneficial properties of Vulcan, its microporosity (47% of micropores with a pore size less than 2 nm in diameter) limits fuel cell performance because the pores are not easily accessible by the electrolyte. 11,12 Mesoporous carbons on the other hand when used as supports of Pt catalysts for direct methanol fuel cells (DMFC) showed improved performance compared with microporous carbons. The results were attributed to enhanced diffusion of reactants through the mesoporous network. 6,13 Similarly, mesopores (2–50 nm) in carbon supports such as Ketjen black not only shield catalytic

Received: February 13, 2023 Accepted: June 13, 2023 Published: June 27, 2023





Scheme 1. Schematic of HPC Synthesis Showing the Various Steps Involved



nanoparticles from the ionomer but also protect against particle migration and coalescence. Finally, the presence of macropores in the support facilitates gas diffusion and it is beneficial to the overall performance.

In this context, hierarchical porous carbons (HPCs) are attractive model systems for investigating the impact of structural characteristics on electrochemical performance, due to the combination of high surface area with the ability to control both the type, as well as the size of porosity. Because of this combination, HPCs have been suggested as materials of choice for energy storage-related applications such as supercapacitors and electrodes for lithium batteries. 15-18

In this paper, we study a series of HPCs with high surface area and well-defined mesoporosity as catalyst supports for alkaline fuel cells. The latter are gaining considerable momentum as an alternative to acidic polymer electrolyte membrane fuel cells because of their ability to use nonprecious metal catalysts.3 We explore how the structural and morphological characteristics of HPCs affect the deposition of the Pt nanoparticles and the overall performance of the resulting electrocatalysts. More specifically, we focus on how the mesoporosity influences the size and size distribution of Pt particles and correlate these results to their ECSA and ORR activity. By using a well-established protocol developed previously in our group that enables the controlled synthesis of HPCs with tunable and well-defined mesoporosity, we synthesized a series of model HPCs (Scheme 1), investigated their effect on catalyst nanoparticle deposition, and studied their electrocatalytic performance. The performance of the electrocatalysts is compared with state-of-the-art electrocatalysts based on a microporous commercial carbon (TEC10E50E) that is widely used in fuel cell systems.

Since a common strategy for improving the performance of an electrocatalyst is to increase its electronic conductivity, we have also synthesized an HPC containing graphene (referred to as HPC-GN) by adding graphene nanoplatelets during the synthesis. As previously reported, carbon composites containing graphene, graphene oxide, and carbon nanotubes exhibit higher electrocatalytic activity. Following Pt deposition, the HPC-GN hybrid was characterized and its performance was evaluated and compared to the other systems. Altogether, this work represents a systematic study of exploring how

chemical, structural, and morphological features affect the mechanism of catalyst deposition and provides further insights into the performance of these systems as electrocatalysts in alkaline membrane fuel cells.

EXPERIMENTAL SECTION

Synthesis of HPCs. HPCs were fabricated by an ice-templating method developed previously. 15-18 A second thermal annealing step was also performed to increase their electrical conductivity. 23,24 ice-templating method was used to produce HPCs with different mesopore sizes ranging from 4 to 20 nm. For convenience, HPCs synthesized as described below are denoted as HPC-xx, where xrepresents the average colloidal silica nanoparticle size (nm) used as a template. Scheme 1 describes the synthesis steps used. In brief, sucrose (Sigma-Aldrich) and the appropriate silica nanoparticle colloidal dispersion (4 nm: 15 wt % - Alfa Aesar; 12 nm: LUDOX HS-30, 30 wt % - Sigma Aldrich; and 20 nm: 40 wt % - Alfa Aesar) are mixed in a 1:1 weight ratio. The resulting dispersion was freezedried and then calcined at 1000 °C for 3 h under nitrogen flow. An etching step using 3 M NaOH was followed to remove the silica template. A post thermal treatment at 900 °C for 30 min under nitrogen flow was used following the removal of silica to increase the electrical conductivity of the samples. The HPC graphene hybrid system, denoted as HPC-GN, was prepared by adding graphene nanoplatelets (GN), (Sigma-Aldrich) to the initial sucrose/silica nanoparticle mixture (using 12 nm silica particles as template) and keeping the sucrose/GN ratio as 60/40 wt %. After the GN addition, the same procedure was followed as described above for the other samples.

Preparation of HPC-Supported Pt Electrocatalysts. For the deposition of the Pt catalyst onto the HPC supports, a modified wet impregnation method was followed. Briefly, the support was immersed into a solution of the metal precursor and the mixture was freeze-dried. Specifically, to achieve a Pt loading of ~40 wt % in the electrocatalyst, 5 mL of an 8 wt % chloroplatinic acid solution (Sigma-Aldrich) was added to 250 mg of HPC dispersed in 10 mL DI water, sonicated for 10 min, and immersed into liquid nitrogen until solidified. A freeze dryer was used to sublime the ice crystals. The mixture after freeze-drying was transferred to a crucible and heated at 225 °C (heating rate of 2 °C/min) under a constant flow using a mixture of 6% $H_2/94\%$ N_2 for 2 h.

Characterization Methods. Surface morphology, microstructure, and chemical composition were investigated by scanning electron microscopy (SEM) and energy dispersive X-ray spectroscopy (EDS) using a Zeiss Gemini 500 Scanning Electron Microscope with operating voltages between 1 and 5 keV. Nitrogen adsorption

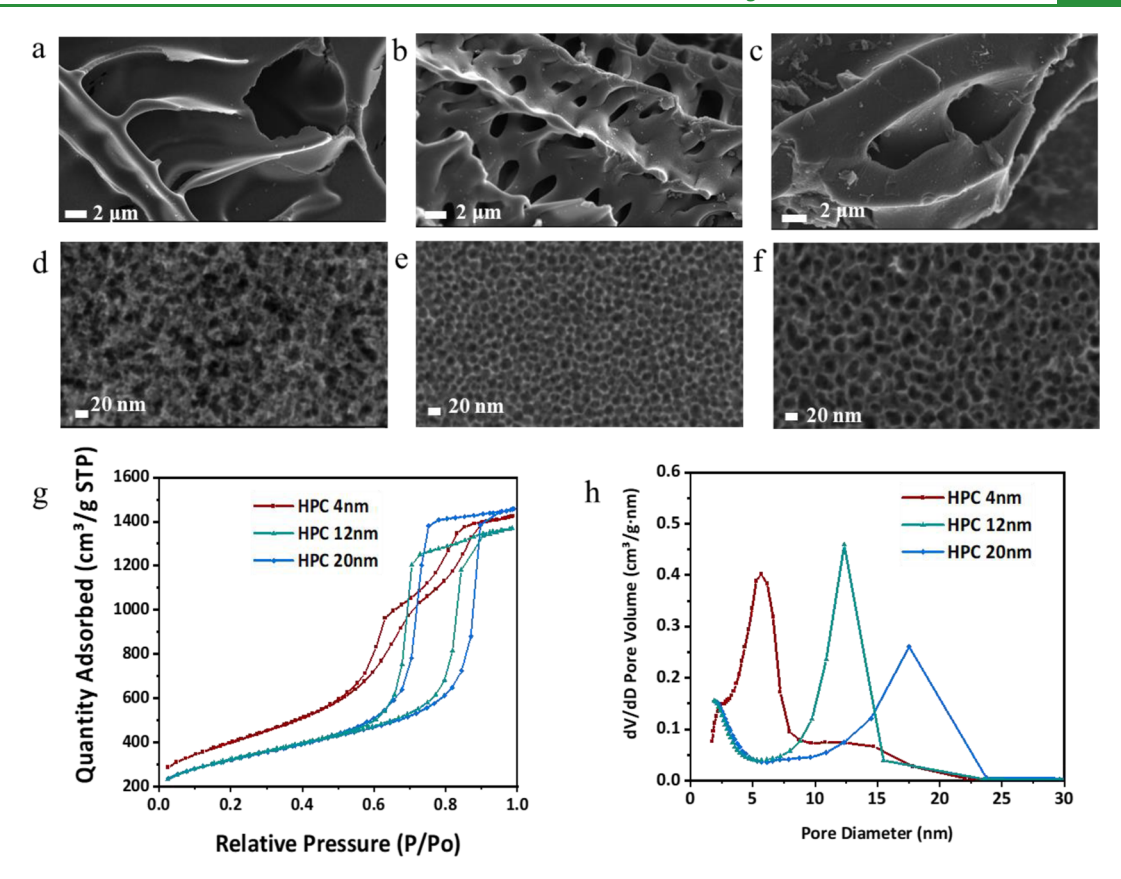


Figure 1. SEM images of HPC-4 (a, d), HPC-12 (b, e), and HPC-20 (c, f). The corresponding nitrogen adsorption isotherms (g) and BJH-derived pore size distributions (h) for HPC-4, HPC-12, and HPC-20.

isotherms were acquired on Micromeritics ASAP 2460 analyzer at 77 K. Elemental composition and electronic structure were estimated using powder samples on silicon substrates via energy-dispersive X-ray spectroscopy using an Oxford Instruments Ultim Max detector, Zeiss Gemini 500 Scanning Electron Microscope, (aperture: 30 μ m, accelerating voltage: 10 kV). X-ray photoelectron spectroscopy (XPS) was performed using an ESCA 2SR XPS operating at 10⁻⁹ Torr. The samples in powder form were deposited on copper tape. Survey spectra were collected at 200 eV and high resolution at 50 eV. Thermogravimetric analysis (TGA) measurements were performed in the air on a TA Instruments Q500 thermogravimetric analyzer using a heating rate of 5 °C/min. Electrical conductivity was measured using a custom made 4-probe setup as described elsewhere. 16 Scanning transmission electron microscopy (STEM) images were obtained on a FEI Tecnai F-20 S/TEM with a Schottky field emission gun at 200 kV. The samples in powder form were dispersed in ethanol, dropcasted onto lacey carbon TEM grids, and air-dried. AFM measurements were conducted in peak force quantitative nanomechanical mapping on a Multimode 8, Nanoscope 6 (Bruker), using scanasystair probes (Bruker). The prepared inks were deposited onto silicon wafers (p-type Si, single side polished, purchased from Pure Wafer) by drop casting. The deflection sensitivity of the photodetector was calibrated by acquiring approach-retract curves on a sapphire sample and the spring constant of the cantilever was calibrated using the thermal tuning method.

Electrochemical Characterization. Electrode preparation — thin film electrodes of ~40% Pt loaded HPC-4, HPC-12, HPC-20, and HPC/GN were prepared by drop-casting a suspension 10 μ L of an ink containing 20 mg of Pt/HPC in 4.1 mL of n-propanol on a 5 mm diameter glassy carbon rotating disk electrode (RDE) and allowed to dry. To improve the film quality, 114 μ L of 2 wt. % alkaline ionomer QAPPT (quaternary ammonium poly(N-methyl-piperidine-co-p-terphenyl) in DSMO was added. To ensure homogeneity, the suspension was tip-sonicated in an ice bath for 30 min. The glassy

carbon RDE was polished with 0.05 μ m alumina suspension and bath sonicated three times in nanopure water. The electrodes contained 0.1 mg Pt/cm². Prior to testing, the films were visually inspected for defects.

Cell preparation - prior to electrochemical measurements, all glassware and electrodes were cleaned well to remove cationic, anionic, and organic impurities. The glass cell was boiled in 1 M nitric acid, rinsed, followed by triple boiling in nanopure water, and finally rinsed 8 times with nanopure water. The cleanliness of the cell was verified by comparing it to previously acquired data on polycrystalline Pt.26

RDE measurements - electrochemical measurements were taken with a SP300 Biologic potentiostat in a glass (Pine Instruments) cell. First, a 0.1~M~KOH~(99.99%~purity,~Sigma-Aldrich) electrolyte was prepared. Next, the working electrode was mounted onto a Pine Instruments rotator and immersed into the electrolyte. An Ag/AgCl reference electrode (saturated KCl) and Pt wire counter electrode were used. The Ag/AgCl electrode was calibrated against the reversible hydrogen electrode (RHE) in a H₂-saturated 0.1 M KOH solution by measuring HOR/HER currents at a Pt RDE.

The Pt/HPC film was activated by cycling between 0 and 1.2 V vs RHE for 40 cycles at 200 mV/s. The electrochemical surface area (ECSA) was determined by hydrogen adsorption. A blank cyclic voltammetry (CV) (Ar-saturated) from 0.08 to 1.12 V vs RHE at 5 mV/s was taken. The activity of the Pt/HPC toward oxygen reduction reaction (ORR) was measured in O2-saturated 0.1 M KOH, from 0.08 to 1.12 V vs RHE at 5 mV/s and 1600 rpm. The method was repeated for the commercial product Pt/C (TEC10E50E) supplied by Tanaka Kikinzoku (TKK).

Membrane electrode assembly (MEA) preparation and measurements - For MEA testing, 7.5 mg of the electrocatalyst sample was placed in a glass and 1.5 mL of n-propanol was added followed by 75 μL of 2 wt % solution of QAPPT ionomer in DMSO. The mixture was sonicated for ~10 min with occasional shaking to form a uniform

suspension. This mixture was used as the catalyst ink for the anode. The cathode ink was made by using the same process but with 6 mg of 60 wt % Pt/C purchased from the fuel cell store and the same amount of propanol and ionomer. The catalyst inks were sprayed onto a membrane of QAPPT using an airbrush. The airbrush was rastered over a 1.5 cm × 1.5 cm square using a modified 3D printer until all the ink was sprayed onto the membrane. This process resulted in \sim 0.95 mg Pt/cm² on the anode and \sim 1.15 mg Pt/cm² on the cathode after accounting for mass losses during the spraying. Once both sides of the membrane were sprayed, it was soaked in 0.1 M KOH overnight (~16 h) at 70 ° C then soaked in deionized (DI) water for 1 min before being placed into the fuel cell. The fuel cell was purchased from Scribner Associates Inc. and Sigracet 28 BC carbon paper was used as the gas diffusion electrodes. The cell and inlet gases were heated to 80 °C and the system had a relative humidity of 100%. A break-in process was performed by increasing the current in steps, starting with 5 mA and then increasing the current steps by ~8% of the total current until the maximum step size of 30 mA was reached. Then a step size of 30 mA was used until the cell voltage dropped to 0.3 V. 50 mA step sizes were used to scan back to the open circuit. A final, fast scan was then recorded with step sizes starting at 5 mA and increasing by ~15% of the total current until reaching the maximum step size of 50 mA.

RESULTS AND DISCUSSION

Structural and Chemical Characterization of HPCs and Pt/HPCs and Effect on Conductivity. HPC-4, HPC-12, and HPC-20 were synthesized as reported previously 15 except an extra thermal treatment step was performed to increase the electrical conductivity of the HPC supports.²⁴ The additional thermal treatment does not alter the porosity or the structural characteristics of the materials, as confirmed by SEM and nitrogen porosimetry (Figure S1).²⁷ However, this extra thermal treatment does affect the chemical composition of the samples, as shown by both XPS and EDS. As the XPS and EDS spectra (Figure S2) show, the oxygen content is decreased by about 50% after the second thermal treatment for all samples. This difference seems consistent for both the surface (determined by XPS), as well as the bulk chemical composition, as shown by EDS. The change in the chemical composition is attributed to the removal of oxygen-containing groups during the second pyrolysis, which eventually leads to an increase in the conductivity of the samples as summarized in Table S1. In all cases, an almost two-fold increase in electronic conductivity is observed with values increasing from 2-5 to 6-9 S/cm after the heat treatment with the graphene-containing sample reaching a value of 32 S/cm (see below).

As the SEM images show (Figure 1a-c), all HPCs possess distinct macropores ranging in size from 2 to 4 μ m. In addition, they show (Figure 1d-f) an extensive network of mesopores with a pore size corresponding to the size of the silica nanoparticles used as the hard template (recall HPC-4, HPC-12, and HPC-20 refer to samples synthesized using silica particles with a diameter of 4, 12, and 20 nm as a template, respectively) validating the high fidelity of the templating process. Consistent with these features, the N2 isotherms for HPC-12 and HPC-20 (Figure 1g) are type IV with a type H1 hysteresis loop consistent with well-defined pores.²⁸ For HPC-4, the hysteresis loop shows a two-step desorption process, which is consistent with the presence of two kinds of mesopores with different diameters (or a potentially partially plugged system).²⁹ All HPCs show high specific areas in excess of 1000 m²/g (Table S2). The mesopore size and distribution, as well as the total pore volume of the samples, were determined from the adsorption part of the isotherms using the

Barrett–Joyner–Halenda (BJH) model. HPC-4 shows a bimodal distribution of pores with the majority centered around 4 nm and a small fraction with a size of 12 nm consistent with the shape of the adsorption isotherm (vide supra). While HPC-12 and HPC-20 show a monomodal pore size distribution the breadth of the peak suggests a broader size distribution. Compared to HPCs, HPC-GN has a lower surface area (\sim 420 m²/g) with well-defined mesopores centered around 12 nm and as with the other samples consistent with the size of the silica nanoparticles used as a template (Figure S3a,b). Despite the lower surface area, the conductivity of this sample is higher compared to the materials without GN, with the conductivity reaching 32 S/cm after the second thermal treatment as mentioned earlier.

Next electrocatalysts were prepared based on the above supports using a wet impregnation method. The loading of the catalyst was verified by TGA, while EDS and XPS were also employed not only to confirm the weight percentage of Pt on the support but also to characterize the elemental composition of all samples. As shown in Figure S4, the Pt loading of all samples were similar (40 \pm 3 wt %) and comparable to the commercially available electrocatalyst (Pt loading 45 \pm 2.5 wt %). Moreover, all samples were more or less similar in terms of their overall chemical composition and comparable to the commercial Pt/C sample with carbon and oxygen content ranging from 89–92% to 4–6%, respectively.

Following the Pt deposition and before electrochemical testing all samples were characterized fully to determine possible changes caused by the impregnation process. Table S3 shows the BET surface area and pore volume of the HPCs after the Pt deposition, as determined by nitrogen adsorption. For Pt/HPCs, the surface area and pore volume of all sample decreases to about half of their initial value after Pt deposition. For example, the surface area of HPC after Pt deposition (Pt/ HPC-4) decreases from 1390 to 670 m²/g. The corresponding mesopore volume before and after Pt deposition is 2.27 and 1.08 cm³/g, respectively. Tables S2 and S3 summarize the results for all samples. Nevertheless, the surface area of all samples is still higher than that of the state-of the-art commercial Pt/C used as a control. In addition, mesopores are the major contributors of porosity in all the HPCs with microporosity being only a very small fraction (Tables S2 and S3). The surface area of the commercial sample (Pt/C) is \sim 400 m²/g and it is due mostly to micropores (Table S3). Therefore, the HPCs differ from the commercial control sample in terms of both the size of the surface area, as well as the type of porosity present. The adsorption isotherms suggest that all the HPC systems retain their mesoporous nature (Figure S5a) after Pt deposition. The pore volume decreased after Pt deposition but the mesopore size and size distribution were not affected (Figures S5b and S6). For comparison, the surface area of the HPC-GN hybrid, after Pt impregnation, decreased to 220 m²/g while it retained a significant amount of mesoporosity (Figure S7), similar to the Pt/HPC systems discussed above.

Study of Pt Catalytic Particles. The size and size distribution of the catalytic nanoparticles deposited on the surface of the support, along with the possible formation of aggregates during operation, dramatically influences the overall performance of an electrocatalyst^{30,31} with the specific conditions of the impregnation step greatly affecting the particle size of the final catalyst.³² Another important parameter is the metal loading on the support, with increasing

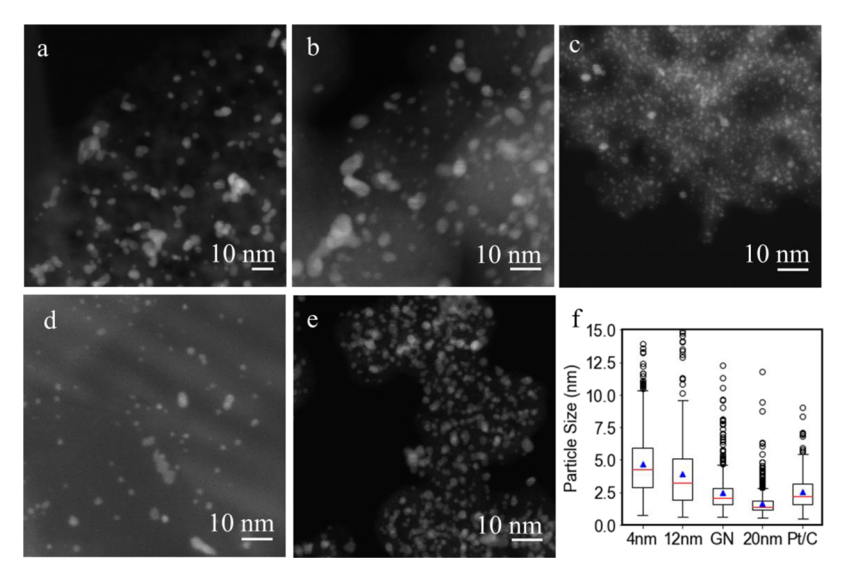


Figure 2. HAADF-STEM images of Pt/HPC (a) Pt/HPC-4, (b) Pt/HPC-12, (c) Pt/HPC-20, (d) Pt/HPC-GN, and (e) Pt/C (scale bars 10 nm). (f) Boxplots of PSD of more than 400 particles per group. Red lines within boxes indicate medians, and blue triangles denote mean values. Whiskers are drawn within the 1.5 interquartile range. Empty circles depict outliers.

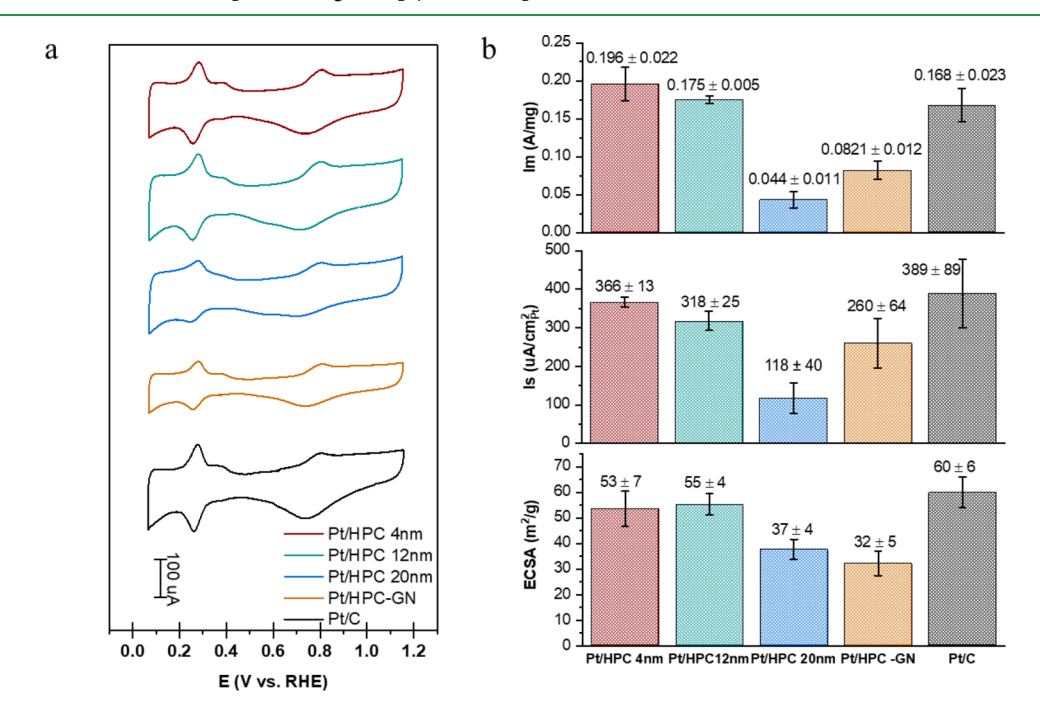


Figure 3. Electrochemical characterization using rotating disk electrodes. (a) Cyclic voltammograms and (b) mass-specific activity, area-specific activity, and electrochemical surface area (from top to bottom) for Pt/HPC-4, Pt/HPC-12, Pt/HPC-20, Pt/HPC-GN, and Pt/C.

loading leading to larger particle sizes and shorter interparticle distances, both of which affect catalytic activity.³³ The differences in the catalyst particle size, as well as its adhesion on the support, are often attributed to the chemical nature, e.g., surface functional groups of the support that are present prior to the catalyst loading. In addition to the available surface area, the density of functional groups on the surface controls the nucleation of catalyst particles, preventing agglomeration and resulting in particles of smaller size and narrow size distribution.³⁴

The size and size distribution of the Pt nanoparticles on various supports was determined from high-angle annular dark field scanning transmission electron microscope (HAADF-STEM) images using a detailed statistical analysis (Table S4).

As shown in Figure 2, the mean size of Pt on HPC-4, HPC-12, and HPC-20 is 4.7, 3.9, and 1.6 nm, respectively. Interestingly, the smaller the pore size of the carbon support the larger the size of the deposited Pt nanoparticles. Pt/HPC-4 and Pt/HPC-12 show a similar size distribution. Pt/HPC-20 exhibits a narrower size range relative to all other systems (i.e., the Pt nanoparticles are much more uniform compared to the rest). We note that the size of the Pt/HPC-20 is smaller and more uniform compared to the commercial Pt/C sample.

As noted above, the size of the deposited nanoparticles is influenced by the structural/morphological and chemical characteristics of the support. The three supports used (HPC-4, HPC-12, and HPC-20) exhibit comparable surface areas and pore volumes but different pore sizes. EDS and XPS

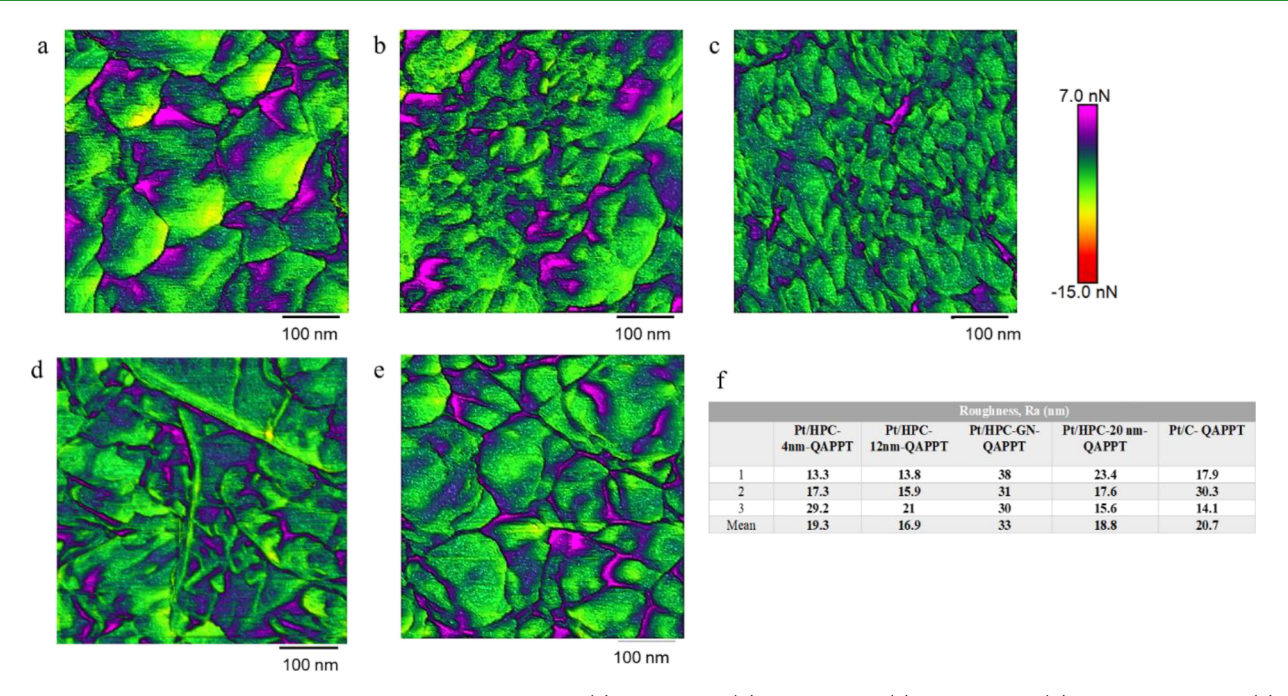


Figure 4. AFM adhesion force maps for electrodes prepared using (a) Pt/HPC-4, (b) Pt/HPC-12, (c) Pt/HPC-20, (d) Pt/HPC-GN, and (e) Pt/C. The roughness values are summarized in a Table in (f). All electrodes were prepared by adding the same amount of QAPPT to the ink containing the various electrocatalysts.

analysis also suggest somewhat similar chemical nature for the three HPCs (Figure S2). In addition to the same chemical composition obtained from the XPS survey spectra, the deconvolution of the C1s spectra shows the presence of similar chemical groups for all the supports. For example, the percentage of C–C (sp²) and C=C (sp³) groups is around 67% while those of oxygen containing groups (C–O, C=O and O–C=O) is ~28%. Finally, Raman spectroscopy shows similar spectra with an $I_{\rm D}/I_{\rm G}$ ratio of about 1. Since the deposition process and the amount of catalyst precursor used are also similar for all HPC samples, what is the reason for the different Pt nanoparticle size?

Based on the size of the precursor used, access to the pores of the support is not expected to be an issue.³² The observed trend in our system (larger pores lead to smaller Pt catalyst sizes) is contrary to previous reports, where the size of the particles scales with the size of the pores. We suggest that the particle growth is controlled by the mesoporous network as reported previously for mesoporous carbons.²⁷ In addition, preliminary measurements using a series of liquids suggest that HPC-4 and HPC-12 possess similar hydrophilicity but HPC-20 is more hydrophobic. Recall that the size and size distribution of Pt deposited on HPC-20 is much smaller compared to HPC-4 and HPC-12. These differences in hydrophilicity/hydrophobicity (i.e., surface and interfacial surface energies) of the support might be responsible for the observed size differences. Further experiments are in progress, and we plan to communicate all findings in a follow up publication.

Interestingly, the use of HPC-GN decreases the particle size of the catalyst. As shown in Figure 2d, the mean size of Pt particles for Pt/HPC-GN is 2.5 nm, comparable to the catalyst particle size of commercial Pt/C and lower than that of Pt/HPC-12, which has a similar pore size. Again, we note that the smaller size and size distribution is consistent with a more hydrophobic nature of the HPC-GN sample.

Electrochemical Activity of Pt/HPC Catalysts. The ECSA of all Pt systems was determined by the hydrogen adsorption method. First, a CV is performed in an Arsaturated 0.1 M KOH solution and the results are shown in Figure 3a. Then, the negative going potential scan is integrated from 0.4 to 0.075 V vs RHE, after correcting for double layer capacitance. The result is the charge of hydrogen adsorption, $Q_{\text{H-adsorption}}$, in eq 1, where L_{Pt} is the loading of Pt on the glassy carbon electrode (mg_{Pt}), and 210 μ C cm_{Pt}⁻² is the charge of hydrogen adsorption on polycrystalline Pt. The ECSA plots in Figure 3b are normalized to Pt loading, as calculated using eq 1.

$$ECSA_{Pt}(m^{2}g_{Pt}^{-1}) = \left[\frac{Q_{H-adsorption}(C)}{210 \ \mu C \ cm_{Pt}^{-2} \ L_{Pt}(mg_{Pt})}\right]10^{5}$$
(1)

The variation of ECSA among the Pt/HPC samples is linked directly to the Pt particles and to their size. Previous reports have suggested that ECSA is inversely proportional to the catalyst particle size. 35 The ECSA for Pt/HPC-4 and Pt-HPC-12 are comparable (53.7 and 55.4 m_{Pt}^2/g_{Pt} respectively). The mean sizes of the catalyst particles for these samples are also comparable $(4.7 \pm 2.7 \text{ and } 3.9 \text{ nm} \pm 2.7, \text{ respectively}).$ However, for Pt/HPC-20, where the mean size of the Pt catalyst particles is 1.6 nm \pm 0.8, the ECSA is $37.4 \text{m}^2_{\text{Pt}}/g_{\text{Pt}}$ significantly lower compared to the other supports. A possible explanation for the lower value might be the instability of the Pt nanoparticles when their size is smaller than 2 nm.³¹ For example, studies of Pt on hollow graphitic spheres, showed that small catalytic particles do not retain their initial ECSA and degrade rapidly.³⁶ Comparing the Pt/HPC-GN, where the size of the catalyst particles is around 2.5 \pm 1.5 nm, similar to the commercial Pt/C, the two systems show significantly different ECSA values (32.3 and 60 m_{Pt}^2/g_{Pt} respectively). The differences in these two systems might be related to the different types of pores present (i.e., mesopores for the Pt/

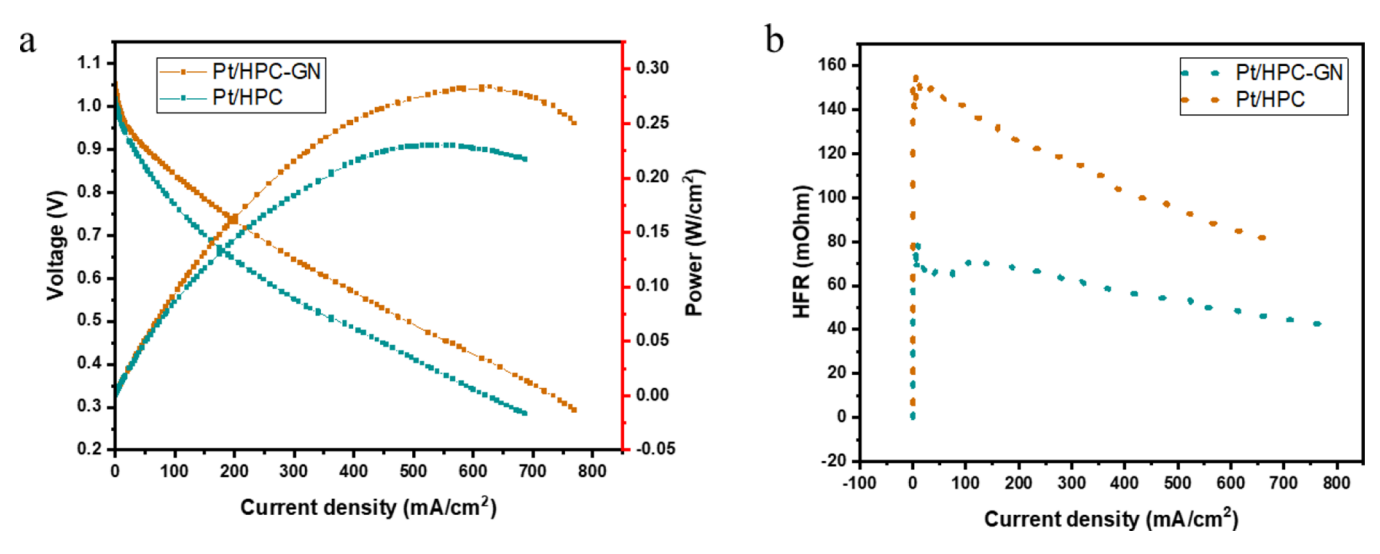


Figure 5. Membrane electrode assembly, MEA, results in an alkaline fuel cell: (a) power and current density for Pt/HPC-12 and Pt/HPC-GN and (b) MEA conductivity.

HPC-GN and micropores for the commercial Pt/C), as well as the differences in the film roughness measured by AFM (see below).

There is a current debate regarding the effect of Pt particle size on the ORR activity. For example, Yano et al. studied the ORR of Pt supported on carbons with particle sizes ranging from 1 to 5 nm and found no particle size dependence on the ORR activity.³⁷ On the other hand, there have also been reports showing a direct correlation of ORR activity with catalyst size with larger catalytic particles showing higher specific ORR activity.^{34,38} The optimum size for the maximum of mass activity ranges between 3 and 5 nm with the ideal size being around 4 nm.³⁵ Moreover, there are reports showing that an increase in particle size can result in stronger adsorption of oxygenated species and thus improved ORR.³⁵

The ORR activities were compared in a 0.1 M KOH $\rm O_2$ -saturated electrolyte by using a RDE at 1600 RPM. The blank CV in Ar was subtracted from the ORR current to remove artifacts of hydrogen adsorption and Pt oxidation. The kinetic current at 0.9 V vs RHE was normalized to ECSA and Pt loading (Figure 3) and the kinetically limited current I_k was calculated using eq 2:

$$I_{k}(A) = \frac{I_{lim}(A) \times I(A)}{I_{lim} - I}$$
(2)

The mass activity for HPC-4, HPC-12, and HPC-20 decreases from 0.196 \pm 0.022 to 0.175 \pm 0.005 to 0.044 \pm 0.011A/mg_{Pt}. In other words, the activity decreases as the Pt catalyst size decreases, consistent with the view that an increase in the Pt particle size can be beneficial for ORR catalysis. The specific activity for Pt/HPC-GN was lower (0.082 \pm 0.012 A/mg_{Pt}), even though the higher conductivity of that support was expected to lead to higher values. We hypothesize that other features of the electrode including the uniformity and roughness of the film could also affect the RDE results.

To that end, we used atomic force microscopy (AFM) to characterize the films after deposition. In addition to roughness, AFM can provide information about the uniformity and distribution of the different components including the ionomer. As Figure 4 shows, the films do not appear uniform with respect to the distribution of the ionomer (purple color

phase) despite the similar fabrication process and amount of material used. We note that Pt/HPC-4 is more similar in morphology with the commercial Pt/C catalyst. The roughness of Pt/HPC-GN is consistently higher than that of the other HPC-based catalyst systems, potentially affecting its performance. It is also possible that the performance of electrocatalysts based on HPC-4, HPC-12, and HPC-20 is affected by the differences in the distribution of the ionomer in the films. While all films contain the same amount of ionomer (~10 wt %), the film based on HPC-4 shows larger carbon domains and surface enrichment of the ionomer. Both the size of the domains and the ionomer concentration on the surface decrease as we consider films based on HPC-12 and HPC-20 (Figure 4).

MEAs were fabricated and tested in an alkaline polymer fuel cell to determine the performance of these systems under more realistic conditions. Even though RDE studies are useful for quantifying the activity of a catalyst, they are limited in that they do not capture all aspects of the catalyst's performance. For example, one such issue is the conductivity of the support, since very thin films of catalysts are typically used in RDE experiments minimizing the effect of electrode resistance. In addition to resistance, mass transport may affect the MEA performance.⁴⁰ Consistent with the above, the Pt/HPC-GN system outperformed the Pt/HPC-12 sample in fuel cell testing. In the fuel cell, the catalyst/support layer is much thicker, and HPC systems with lower conductivity thus exhibit higher series resistance. Both the activity and power density are higher for the more conductive system. The Pt/HPC-GN sample shows a peak power density of 0.28 W/cm² at a current density of about 630 mA/ cm² and a maximum current density of 770 mA/ cm². The corresponding values for the HPC without graphene are 0.23 W/cm² at 520 mA/ cm² and a maximum current density of 695 mA/cm² (Figure 5a). Consistent with the above, the Pt/HPC-GN systems show lower high frequency resistance compared to the Pt/HPC-12 (Figure 5b).

CONCLUSIONS

Using a series of model supports based on HPCs, we show that the size of the pores plays a dominant role and controls the growth of the catalyst particles and, thus, their electrochemical performance. An inverse relation between pore diameter and the size and size distribution of the deposited catalyst was observed in the Pt/HPC systems with similar catalyst loading. RDE experiments showed that larger particles had higher specific ECSA and ORR activity. In addition, the HPC supports with larger particle sizes showed similar activity with the commercial Pt/C system although the particle size of the catalyst differs. Furthermore, while the ORR activity of the graphene containing HPC was lower compared to an HPC of similar pore size the MEA performance of the former in terms of current and power density is better because of its much higher conductivity. The study using these model support systems provides new insights and the new mechanistic understanding might pave the way for performance improvements in practical fuel-cell applications.

ASSOCIATED CONTENT

Solution Supporting Information

The Supporting Information is available free of charge at https://pubs.acs.org/doi/10.1021/acsami.3c01935.

XPS, TGA, nitrogen porosimetry, and SEM-EDS results (PDF)

AUTHOR INFORMATION

Corresponding Author

Emmanuel P. Giannelis — Department of Materials Science and Engineering, Cornell University, Ithaca 14853 New York, United States; Email: epg2@cornell.edu

Authors

- Georgia Potsi Department of Materials Science and Engineering, Cornell University, Ithaca 14853 New York, United States
- Yu-Han Joseph Tsai Department of Materials Science and Engineering, Cornell University, Ithaca 14853 New York, United States
- Austin Reese Department of Chemical and Biomolecular Engineering, Cornell University, Ithaca 14853 New York, United States
- Dasol Yoon Department of Materials Science and Engineering, Cornell University, Ithaca 14853 New York, United States; ⊚ orcid.org/0000-0003-2284-7010
- Jeremy L. Hitt Department of Chemistry, University of Pennsylvania, Philadelphia, Pennsylvania 19104, United States
- Antonios Kouloumpis Department of Materials Science and Engineering, Cornell University, Ithaca 14853 New York, United States; orcid.org/0000-0002-8738-3141
- Jin Suntivich Department of Materials Science and Engineering, Cornell University, Ithaca 14853 New York, United States
- David A. Muller School of Applied and Engineering Physics and Kavli Institute at Cornell for Nanoscale Science, Cornell University, Ithaca 14853 New York, United States
- Thomas E. Mallouk Department of Chemistry, University of Pennsylvania, Philadelphia, Pennsylvania 19104, United States; orcid.org/0000-0003-4599-4208

Complete contact information is available at: https://pubs.acs.org/10.1021/acsami.3c01935

Author Contributions

E.P.G. conceived the project; E.P.G., J.S., T.E.M., and D.A.M. guided the project; G.P. and Y.J.T. synthesized and characterized the samples; A.R. performed RDE experiments, J.H. performed MEAs testing, D.Y. conducted STEM measurements, and A.K. performed AFM measurements. The manuscript was written with the contributions of all authors. G.P. and Y.J.T. equally contributed to this work.

Notes

The authors declare no competing financial interest.

ACKNOWLEDGMENTS

This work was supported by the Center for Alkaline-Based Energy Solutions (CABES), part of the Energy Frontier Research Center (EFRC) program supported by the U.S. Department of Energy, under Grant DE-SC-0019445. The authors acknowledge support from the Cornell Energy System Institute (CESI). This work made use of SEM, STEM, TGA, and XPS facilities of the Cornell Center for Materials Research Shared Facilities which are supported through the NSF MRSEC program (DMR-1719875).

REFERENCES

- (1) Garland, N.; Benjamin, T.; Kopasz, J. DOE Fuel Cell Program: Durability Technical Targets and Testing Protocols. *ECS Trans.* **2007**, *11*, 923–931.
- (2) Rashidi, S. Progress and Challenges on the Thermal Management of Electrochemical Energy Conversion and Storage Technologies: Fuel Cells, Electrolysers, and Supercapacitors. *Prog. Energy Combust. Sci.* **2022**, *88*, 100966–94681.
- (3) Yang, Y.; Peltier, C. R.; Zeng, R.; Schimmenti, R.; Li, Q.; Huang, X.; Yan, Z.; Potsi, G.; Selhorst, R.; Lu, X.; Xu, W.; Tader, M.; Soudackov, A. V.; Zhang, H.; Krumov, M.; Murray, E.; Xu, P.; Hitt, J.; Xu, L.; Ko, H.-Y.; Ernst, B. G.; Bundschu, C.; Luo, A.; Markovich, D.; Hu, M.; He, C.; Wang, H.; Fang, J.; DiStasio, R. A.; Kourkoutis, L. F.; Singer, A.; Noonan, K. J. T.; Xiao, L.; Zhuang, L.; Pivovar, B. S.; Zelenay, P.; Herrero, E.; Feliu, J. M.; Suntivich, J.; Giannelis, E. P.; Hammes-Schiffer, S.; Arias, T.; Mavrikakis, M.; Mallouk, T. E.; Brock, J. D.; Muller, D. A.; DiSalvo, F. J.; Coates, G. W.; Abruña, H. D. Electrocatalysis in Alkaline Media and Alkaline Membrane-Based Energy Technologies. *Chem. Rev.* 2022, 122, 6117–6321.
- (4) Ejikeme, P. M.; Makgopa, K.; Ozoemena, K. I. Effects of Catalyst-Support Materials on the Performance of Fuel Cells. In *Nanomaterials for Fuel Cell Catalysis*; Ozoemena, S. C., Chen, S., Eds.; Springer: Cham, 2016; pp 517–550.
- (5) Antolini, E. Carbon Supports for Low-Temperature Fuel Cell Catalysts. *Appl. Catal., B* **2009**, *88*, 1–24.
- (6) Yarlagadda, V.; Carpenter, M. K.; Moylan, T. E.; Kukreja, R. S.; Koestner, R.; Gu, W.; Thompson, L.; Kongkanand, A. Boosting Fuel Cell Performance with Accessible Carbon Mesopores. *ACS Energy Lett.* **2018**, *3*, 618–621.
- (7) Padgett, E.; Yarlagadda, V.; Holtz, M. E.; Ko, M.; Levin, B. D. A.; Kukreja, R. S.; Ziegelbauer, J. M.; Andrews, R. N.; Ilavsky, J.; Kongkanand, A.; Muller, D. A. Mitigation of PEM Fuel Cell Catalyst Degradation with Porous Carbon Supports. *J. Electrochem. Soc.* **2019**, *166*, F198–F207.
- (8) Samad, S.; Loh, K. S.; Wong, W. Y.; Lee, T. K.; Sunarso, J.; Chong, S. T.; Wan Daud, W. R. Carbon and Non-Carbon Support Materials for Platinum-Based Catalysts in Fuel Cells. *Int. J. Hydrogen Energy* **2018**, *43*, 7823–7854.
- (9) Dicks, A. L. The Role of Carbon in Fuel Cells. *J. Power Sources* **2006**, *156*, 128–141.
- (10) Zhou, X.; Qiao, J.; Yang, L.; Zhang, J. A Review of Graphene-Based Nanostructural Materials for Both Catalyst Supports and Metal-Free Catalysts in PEM Fuel Cell Oxygen Reduction Reactions. *Adv. Energy Mater.* **2014**, *4*, No. 1301523.

- (11) Lee, K.; Zhang, J.; Wang, H.; Wilkinson, D. P. Progress in the Synthesis of Carbon Nanotube- And Nanofiber-Supported Pt Electrocatalysts for PEM Fuel Cell Catalysis. *J. Appl. Electrochem.* **2006**, *36*, 507–522.
- (12) Fang, B.; Kim, J. H.; Kim, M. S.; Yu, J. S. Hierarchical Nanostructured Carbons with Meso-Macroporosity: Design, Characterization, and Applications. *Acc. Chem. Res.* **2013**, *46*, 1397–1406.
- (13) Joo, S. H.; Pak, C.; You, D. J.; Lee, S.-A.; Lee, H. I.; Kim, J. M.; Chang, H.; Seung, D. Ordered Mesoporous Carbons (OMC) as Supports of Electrocatalysts for Direct Methanol Fuel Cells (DMFC): Effect of Carbon Precursors of OMC on DMFC Performances. *Electrochim. Acta* 2006, 52, 1618–1626.
- (14) Sepp, S.; Vaarmets, K.; Nerut, J.; Tallo, I.; Tee, E.; Kurig, H.; Aruväli, J.; Kanarbik, R.; Lust, E. Enhanced Stability of Symmetrical Polymer Electrolyte Membrane Fuel Cell Single Cells Based on Novel Hierarchical Microporous-Mesoporous Carbon Supports. *J. Solid State Electrochem.* **2017**, *21*, 1035–1043.
- (15) Estevez, L.; Dua, R.; Bhandari, N.; Ramanujapuram, A.; Wang, P.; Giannelis, E. P. A Facile Approach for the Synthesis of Monolithic Hierarchical Porous Carbons-High Performance Materials for Amine Based CO2 Capture and Supercapacitor Electrode. *Energy Environ. Sci.* 2013, 6, 1785–1790.
- (16) Baroud, T. N.; Giannelis, E. P. Role of Mesopore Structure of Hierarchical Porous Carbons on the Electrosorption Performance of Capacitive Deionization Electrodes. *ACS Sustainable Chem. Eng.* **2019**, 7, 7580–7596.
- (17) Sahore, R.; Levin, B. D. A.; Pan, M.; Muller, D. A.; DiSalvo, F. J.; Giannelis, E. P. Design Principles for Optimum Performance of Porous Carbons in Lithium—Sulfur Batteries. *Adv. Energy Mater.* **2016**, *6*, No. 1600134.
- (18) Sahore, R.; Estevez, L. P.; Ramanujapuram, A.; Disalvo, F. J.; Giannelis, E. P. High-Rate Lithium-Sulfur Batteries Enabled by Hierarchical Porous Carbons Synthesized via Ice Templation. *J. Power Sources* **2015**, 297, 188–194.
- (19) Huang, B.; He, Y.; Wang, Z.; Zhu, Y.; Zhang, Y.; Cen, K. High-Performance Pt Catalyst with Graphene/Carbon Black as a Hybrid Support for SO2 Electrocatalytic Oxidation. *Langmuir* **2020**, *36*, 20–27
- (20) Nakano, H.; Li, W.; Xu, L.; Chen, Z.; Waje, M.; Kuwabata, S.; Yan, Y. Carbon Nanotube and Carbon Black Supported Platinum Nanocomposites as Oxygen Reduction Electrocatalysts for Polymer Electrolyte Fuel Cells. *Electrochemistry* **2007**, *75*, 705–708.
- (21) Daş, E.; Kaplan, B. Y.; Gürsel, S. A.; Yurtcan, A. B. Graphene Nanoplatelets-Carbon Black Hybrids as an Efficient Catalyst Support for Pt Nanoparticles for Polymer Electrolyte Membrane Fuel Cells. *Renewable Energy* **2019**, *139*, 1099–1110.
- (22) Ji, Z.; Chen, J.; Pérez-Page, M.; Guo, Z.; Zhao, Z.; Cai, R.; Rigby, M. T. P.; Haigh, S. J.; Holmes, S. M. Doped Graphene/Carbon Black Hybrid Catalyst Giving Enhanced Oxygen Reduction Reaction Activity with High Resistance to Corrosion in Proton Exchange Membrane Fuel Cells. *J. Energy Chem.* **2022**, *68*, 143–153.
- (23) Wang, Y.; Chen, Y.; Lacey, S. D.; Xu, L.; Xie, H.; Li, T.; Danner, V. A.; Hu, L. Reduced Graphene Oxide Film with Record-High Conductivity and Mobility. *Mater. Today* **2018**, *21*, 186–192.
- (24) Ramamoorthy, H.; Buapan, K.; Chiawchan, T.; Thamkrongart, K.; Somphonsane, R. Exploration of the Temperature-Dependent Correlations Present in the Structural, Morphological and Electrical Properties of Thermally Reduced Free-Standing Graphene Oxide Papers. J. Mater. Sci. 2021, 56, 15134–15150.
- (25) Garsany, Y.; Baturina, O. A.; Swider-Lyons, K. E.; Kocha, S. S. Experimental Methods for Quantifying the Activity of Platinum Electrocatalysts for the Oxygen Reduction Reaction. *Anal. Chem.* **2010**, *82*, 6321–6328.
- (26) Sheng, W.; Gasteiger, H. A.; Shao-Horn, Y. Hydrogen Oxidation and Evolution Reaction Kinetics on Platinum: Acid vs Alkaline Electrolytes. *J. Electrochem. Soc.* **2010**, *157*, B1529.
- (27) Galeano, C.; Meier, J. C.; Peinecke, V.; Bongard, H.; Katsounaros, I.; Topalov, A. A.; Lu, A.; Mayrhofer, K. J. J.; Schüth,

- F. Toward Highly Stable Electrocatalysts via Nanoparticle Pore Confinement. J. Am. Chem. Soc. 2012, 134, 20457–20465.
- (28) Groen, J. C.; Peffer, L. A. A.; Pérez-Ramírez, J. Pore Size Determination in Modified Micro- and Mesoporous Materials. Pitfalls and Limitations in Gas Adsorption Data Analysis. *Microporous Mesoporous Mater.* **2003**, *60*, 1–17.
- (29) Shakeri, M.; Khatami Shal, Z.; Van Der Voort, P. An Overview of the Challenges and Progress of Synthesis, Characterization and Applications of Plugged SBA-15 Materials for Heterogeneous Catalysis. *Materials* **2021**, *14*, 5082.
- (30) Gupta, G.; Slanac, D. A.; Kumar, P.; Wiggins-Camacho, J. D.; Kim, J.; Ryoo, R.; Stevenson, K. J.; Johnston, K. P. Highly Stable Pt/ Ordered Graphitic Mesoporous Carbon Electrocatalysts for Oxygen Reduction. *J. Phys. Chem. C* **2010**, *114*, 10796–10805.
- (31) Sandbeck, D. J. S.; Inaba, M.; Quinson, J.; Bucher, J.; Zana, A.; Arenz, M.; Cherevko, S. Particle Size Effect on Platinum Dissolution: Practical Considerations for Fuel Cells. *ACS Appl. Mater. Interfaces* **2020**, *12*, 25718–25727.
- (32) Mäki-Arvela, P.; Murzin, D. Y. Effect of Catalyst Synthesis Parameters on the Metal Particle Size. *Appl. Catal., A* **2013**, *451*, 251–281.
- (33) Pillai, S. R.; Sonawane, S. H.; Gumfekar, S. P.; Suryawanshi, P. L.; Ashokkumar, M.; Potoroko, I. Continuous Flow Synthesis of Nanostructured Bimetallic Pt-Mo/C Catalysts in Milli-Channel Reactor for PEM Fuel Cell Application. *Mater. Chem. Phys.* **2019**, 237, No. 121854.
- (34) Lee, W.-J.; Bera, S.; Kim, C. M.; Koh, E.-K.; Hong, W.-P.; Oh, S.-J.; Cho, E.; Kwon, S.-H. Synthesis of Highly Dispersed Pt Nanoparticles into Carbon Supports by Fluidized Bed Reactor Atomic Layer Deposition to Boost PEMFC Performance. *NPG Asia Mater.* **2020**, *12*, 40.
- (35) Xu, Z.; Zhang, H.; Zhong, H.; Lu, Q.; Wang, Y.; Su, D. Effect of Particle Size on the Activity and Durability of the Pt/C Electrocatalyst for Proton Exchange Membrane Fuel Cells. *Appl. Catal., B* **2012**, 111–112, 264–270.
- (36) Meier, J. C.; Galeano, C.; Katsounaros, I.; Witte, J.; Bongard, H. J.; Topalov, A. A.; Baldizzone, C.; Mezzavilla, S.; Schüth, F.; Mayrhofer, K. J. J. Design Criteria for Stable Pt/C Fuel Cell Catalysts. *Beilstein J. Nanotechnol.* **2014**, *5*, 44–67.
- (37) Yano, H.; Inukai, J.; Uchida, H.; Watanabe, M.; Babu, P. K.; Kobayashi, T.; Chung, J. H.; Oldfield, E.; Wieckowski, A. Particle-Size Effect of Nanoscale Platinum Catalysts in Oxygen Reduction Reaction: An Electrochemical and 195Pt EC-NMR Study. *Phys. Chem. Chem. Phys.* **2006**, *8*, 4932–4939.
- (38) Inaba, M.; Zana, A.; Quinson, J.; Bizzotto, F.; Dosche, C.; Dworzak, A.; Oezaslan, M.; Simonsen, S. B.; Kuhn, L. T.; Arenz, M. The Oxygen Reduction Reaction on Pt: Why Particle Size and Interparticle Distance Matter. ACS Catal. 2021, 11, 7144–7153.
- (39) Morawietz, T.; Handl, M.; Oldani, C.; Friedrich, K. A.; Hiesgen, R. Quantitative in Situ Analysis of Ionomer Structure in Fuel Cell Catalytic Layers. *ACS Appl. Mater. Interfaces* **2016**, *8*, 27044–27054
- (40) Lazaridis, T.; Stühmeier, B. M.; Gasteiger, H. A.; El-Sayed, H. A. Capabilities and Limitations of Rotating Disk Electrodes versus Membrane Electrode Assemblies in the Investigation of Electrocatalysts. *Nat. Catal.* **2022**, *5*, 363–373.